Chemical Science

EDGE ARTICLE

View Article Online
View Journal | View Issue

Cite this: *Chem. Sci.*, 2019, **10**, 1426

All publication charges for this article have been paid for by the Royal Society of Chemistry

F_{10}BINOL-derived chiral phosphoric acid-catalyzed enantioselective carbonyl-ene reaction: theoretical elucidation of stereochemical outcomes†

Jun Kikuchi, Hiromu Aramaki, Hiroshi Okamoto and Masahiro Terada *

Received 13th August 2018
Accepted 17th November 2018

DOI: 10.1039/c8sc03587c

rsc.li/chemical-science

An F_{10}BINOL-derived chiral phosphoric acid was shown to be an effective catalyst for an enantioselective carbonyl-ene reaction of 1,1-disubstituted olefins with ethyl glyoxylate as the common enophile. The perfluoro-binaphthyl skeleton is beneficial not only for adopting high catalytic activity but also for creating an effective chiral environment for enantioselective transformations. Indeed, the reaction afforded enantio-enriched homoallylic alcohols in high yields with high enantioselectivities. Theoretical studies identified that the multi-point C–H···O hydrogen bonds and the π interactions between the substrates and the 6-methoxy-2-naphthyl substituents at the 3,3′-positions of the F_{10}BINOL skeleton play a crucial role in determining the stereochemical outcomes. The significance of the perfluoro-binaphthyl skeleton in achieving the high enantioselectivity was also evaluated through a structural analysis of the catalysts.

Introduction

The development of enantioselective catalysis using a chiral Brønsted acid has evolved into an active research field over the past decades.[1] In particular, BINOL (1,1′-bi-2-naphthol)-derived chiral phosphoric acids **1**, shown in Fig. 1a, have emerged as privileged organocatalysts[2] for a broad range of enantioselective reactions.[3] As the acidity of chiral Brønsted acids is the dominant factor for generating a range of reactive electrophilic species, the development of strong chiral Brønsted acids is crucial to expand the scope of electrophilic species. In general, the modification of the acidic functionality introduced at the 2,2′-positions of the binaphthyl skeleton has been demonstrated to enhance the acidity of chiral Brønsted acid catalysts.[4] The most representative approach is the introduction of a triflyl group to the nitrogen atom of phosphoramide, namely, BINOL derivatives **2**[4a] shown in Fig. 1b, which exhibit higher acidity than parent phosphoric acids **1**. Hence, *N*-triflylphosphoramides **2** have been widely utilized in the reaction of less reactive substrates, such as carbonyl compounds, which have been much less employed as an electrophile in the reaction using chiral phosphoric acids **1** than imine electrophiles, because of the insufficient acidity of parent phosphoric acids **1**. In this context, we previously executed another approach to enhance the acidity of the parent phosphoric acid: we introduced a perfluoroaryl unit, namely, an F_{10}BINOL moiety,[5] as an axially chiral skeleton and developed F_{10}BINOL-derived phosphoric acid catalyst (*R*)-**3**, shown in Fig. 1c, as a highly acidic chiral Brønsted acid catalyst.[6] The efficient catalytic performance of (*R*)-**3** was proved in the imino-ene reaction of *N*-acyl imines with 1,1-disubstituted olefins, a transformation with few enantioselective examples,[7] affording enantio-enriched homoallylamine derivatives in good yields. The strong electron-withdrawing property of the perfluoro-binaphthyl backbone not only increased the acidity of the catalyst[8] but also maintained the structural properties of the axially chiral binaphthyl skeleton originating from parent chiral phosphoric acid **1**. We anticipated that this highly acidic catalyst **3** would function as an effective enantioselective catalyst even in the reaction of carbonyl compounds. Hence, to further validate the high performance of catalyst **3**, we selected a carbonyl-ene reaction as a beneficial candidate.

The enantioselective carbonyl-ene reaction is a powerful and atom-economical[9] method for the preparation of enantio-

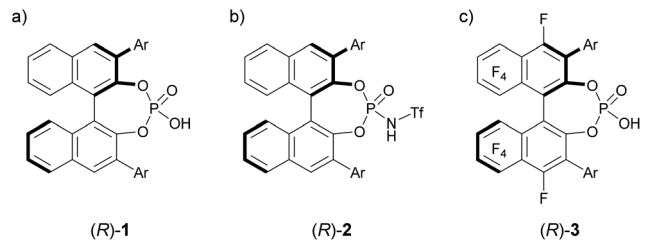

Fig. 1 (a) BINOL-derived phosphoric acid **1** and its analogues (b) **2** and (c) **3**, both of which have higher acidity than **1**.

Department of Chemistry, Graduate School of Science, Tohoku University, Aoba-ku, Sendai 980-8578, Japan. E-mail: mterada@m.tohoku.ac.jp; Fax: +81-22-795-6602; Tel: +81-22-795-6602

† Electronic supplementary information (ESI) available. See DOI: 10.1039/c8sc03587c

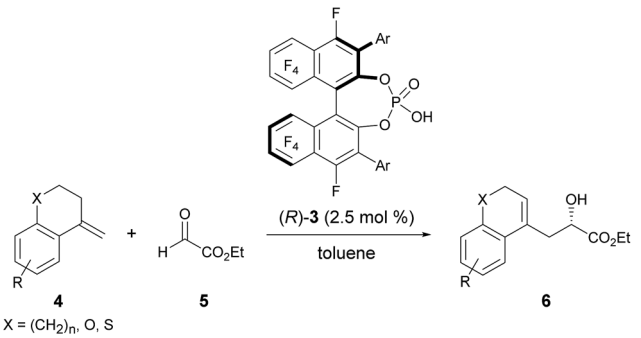

Scheme 1 Enantioselective carbonyl-ene reaction catalyzed by F_{10}BINOL-derived phosphoric acid **3**.

enriched homoallylic alcohols and a number of successful examples using chiral Lewis acidic metal catalysts have been reported to date.[10] However, organocatalytic enantioselective carbonyl-ene reactions are still rarely explored.[11] In fact, successful examples using chiral phosphoric acid derivatives are quite limited. Rueping *et al.* reported an enantioselective carbonyl-ene reaction of 1,1-disubstituted olefins with highly reactive ethyl trifluoropyruvate as the dedicated enophile, using *N*-triflylphosphoramide catalyst **2**.[11a] Meanwhile, List *et al.* recently achieved an enantioselective intramolecular carbonyl-ene cyclization.[11b] Although, in these reports, chiral phosphoric acid derivatives have been successfully employed as the catalyst in the carbonyl-ene reaction, a specific reaction system, such as a dedicated enophile or an intramolecular process, is requisite. In order to demonstrate the notable performance of F_{10}BINOL-derived phosphoric acid (*R*)-**3** as a highly acidic chiral Brønsted acid catalyst,[8] we herein report an intermolecular carbonyl-ene reaction of 1,1-disubstituted olefins **4** with ethyl glyoxylate **5** as the common enophile in the presence of (*R*)-**3** (Scheme 1). The reaction provided homoallylic alcohol products **6** in a highly enantioselective manner and the origin of the stereochemical outcome was elucidated by theoretical studies. Further detailed structural analysis of the phosphoric acid catalysts led to the identification of the specific properties of the F_{10}BINOL skeleton crucial to achieving the high enantioselectivity.

Results and discussion

Optimization of catalyst structure and reaction conditions

As an initial attempt, the reaction of α-methylenetetralin **4a** with ethyl glyoxylate **5** was performed in the presence of (*R*)-**3a** (Ar = phenyl) in toluene at 0 °C (Table 1, entry 1). The carbonyl-ene reaction proceeded smoothly to afford product **6a** in an acceptable yield albeit with moderate enantioselectivity. To improve the enantioselectivity, the effect of the substituents at the 3,3′-positions of **3** was investigated. The enantioselectivity was improved by using catalysts **3b** and **3c**, which have 4-methoxyphenyl and 2-naphthyl groups, respectively, as the substituents (entries 2 and 3). These results stimulated further screening for electron-rich aryl groups that would generate an efficient chiral environment to improve enantioselectivity. Two

Table 1 Optimization of catalyst structure and reaction conditions[a]

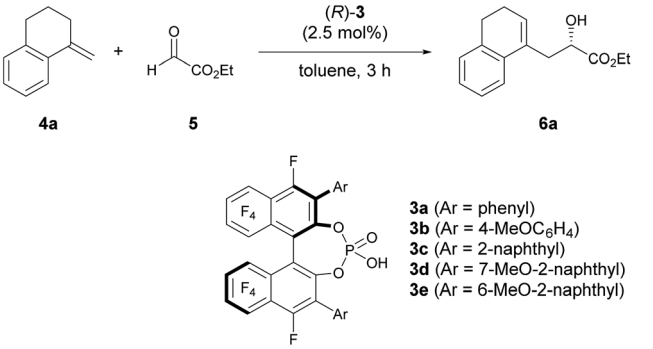

Entry	Catalyst	*T* (°C)	Yield[b] (%)	ee[c] (%)
1	(*R*)-**3a**	0	66	46
2	(*R*)-**3b**	0	94	65
3	(*R*)-**3c**	0	80	69
4	(*R*)-**3d**	0	76	50
5	(*R*)-**3e**	0	83	75
6	(*R*)-**3e**	−20	62	83
7	(*R*)-**3e**	−40	43	85
8	(*R*)-**3e**	−60	51	87
9[d]	(*R*)-**3e**	−60	84	87

[a] Unless otherwise noted, all reactions were carried out using 0.005 mmol of (*R*)-**3** (2.5 mol%), 0.6 mmol of **4a** (3.0 eq.), and 0.2 mmol of **5** in toluene (1.0 mL). [b] Isolated yield. [c] ee was determined by chiral stationary phase HPLC analysis. [d] 0.2 mmol of **4a** and 0.4 mmol of **5** were used.

types of regio-isomeric methoxynaphthyl groups were examined as the more electron-rich aryl substituents than the 4-methoxyphenyl and 2-naphthyl groups. Whereas **3d** with 7-methoxy-2-naphthyl groups resulted in the reduction of enantioselectivity (entry 4), the use of **3e** with 6-methoxy-2-naphthyl groups, in which the position of the methoxy moiety was slightly changed from that in **3d** (7-methoxy-), improved the enantioselectivity (entry 5). Having identified the optimal catalyst as (*R*)-**3e**, further improvement of enantioselectivity was pursued by reducing the reaction temperature (entries 6–8). Gratifyingly, when the temperature was decreased to −60 °C, **6a** was obtained with an increase in enantioselectivity to 87% ee (entry 8), albeit in moderate yield. Further optimization by altering the **4a**:**5** ratio from 3 : 1 to 1 : 2 improved the yield to 84% without any loss of enantioselectivity (entry 9).[12]

Comparison of catalysts

The high potential of F_{10}BINOL-derived phosphoric acid (*R*)-**3** was confirmed by comparing its catalytic efficiency with those of related BINOL-derived phosphoric acids, namely, parent phosphoric acid (*R*)-**1** and its *N*-triflyl derivative (*R*)-**2** (Scheme 2). Indeed, catalyst (*R*)-**1**, having the same 6-methoxy-2-naphthyl substituent, resulted in a considerable decrease in both yield and enantioselectivity. On the other hand, catalyst (*R*)-**2** having the same substituent promoted the reaction smoothly to give **6a** in 83% yield, which was comparable to that of (*R*)-**3e** (84%

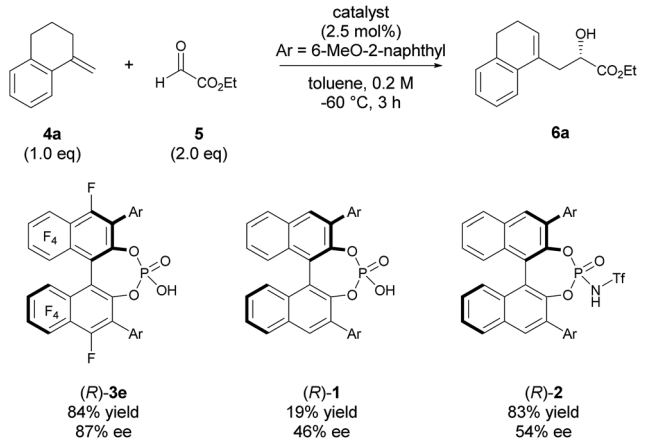

Scheme 2 Comparison of catalysts.

yield), however the enantioselectivity was moderate (54% ee) and comparable to that of (*R*)-**1** having the same BINOL skeleton (46% ee). These results clearly indicate that the introduction of the perfluoro-binaphthyl skeleton leads to not only high catalytic activity but also an effective chiral environment for controlling the stereochemical outcome.

Theoretical studies

We next conducted DFT calculation to elucidate the origin of the stereochemical outcome.[13] Geometry optimization and frequency analysis were performed by the M06-2X/6-31G(d,p) basis set using the Gaussian 16 program.[14–16] Gibbs free energies in the solution phase were calculated using single-point energy calculations at the same level according to the CPCM solvation model (toluene: $\varepsilon = 2.379$) for the optimized structures.[17] A variety of initial structures generated from a series of conformations of 6-methoxy-2-naphthyl substituents attached to the 3,3′-positions of the F_{10}BINOL skeleton were thoroughly explored to identify the energetically favored transition states.[18] The calculated transition states **TS-s** and **TS-r**, affording corresponding products (*S*)-**6a** and (*R*)-**6a**, respectively, are shown in Fig. 2. The Gibbs free energy difference (ΔG) between these two transition states is 1.1 kcal mol^{-1} with **TS-s** resulting in (*S*)-**6a** being energetically favored. The result of the calculation is consistent with the experimental finding that (*S*)-**6a** is obtained as the major enantiomer in the reaction of **4a** with **5** catalyzed by (*R*)-**3e** (Table 1, entry 9).[19]

Further structural analysis of **TS-s** and **TS-r** enabled the identification of the essential factors contributing to the efficient enantioselection. In both transition structures, chiral phosphoric acid **3e** interacts not only with enophile **5** but also with ene-component **4a** through hydrogen bonds: the carbonyl oxygen of enophile **5** interacts through the O···H···O hydrogen bond at the protonation site of the phosphoric acid (P–O<u>H</u>), whereas the vinylic hydrogen of ene-component **4a** interacts through the C–H···O non-classical hydrogen bond at the phosphoryl oxygen (P=O).[20] In the energetically less favorable **TS-r** (Fig. 2b), both **4a** and **5** are inserted perpendicularly between the two naphthyl planes of the catalyst substituents. In contrast, in the energetically more favorable **TS-s** (Fig. 2a), **4a** and **5** are positioned nearly parallel to the two naphthyl planes. In **TS-s** and **TS-r**, the relative positions of the catalyst substituents and the transition structures of the carbonyl-ene reaction are completely different, while these transition states are further stabilized by several noncovalent bond interactions,[21,22] such as C–H···O, C–H···π, and π–π stacking, between the naphthyl substituents and substrates **4a** and **5**. These interactions play crucial roles in determining the relative positions of

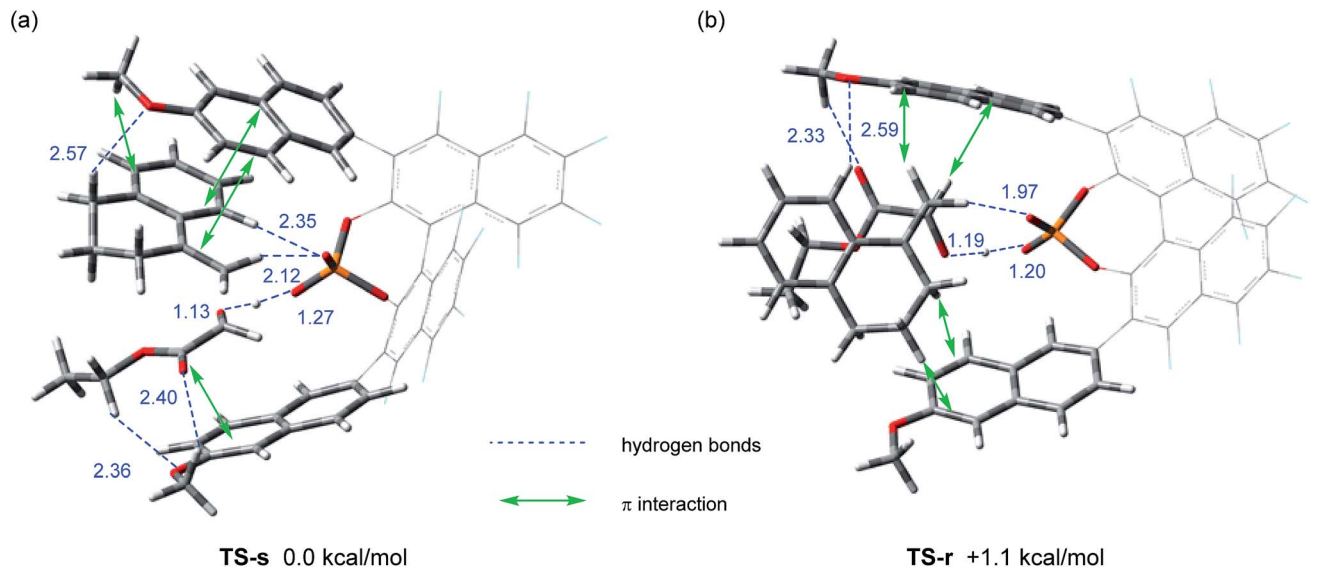

Fig. 2 Transition states in the carbonyl-ene reaction of **4a** with **5** catalyzed by (*R*)-**3e**. Geometries were optimized and characterized using frequency calculations at the M06-2X/6-31G(d,p) level. Relative Gibbs free energies (kcal mol^{-1}) obtained by single-point energy calculations at the same level for the optimized structures with the SCRF method based on CPCM (toluene) are shown. (a) Transition state **TS-s** for the formation of (*S*)-**6a**. (b) Transition state **TS-r** for the formation of (*R*)-**6a**.

the substrates and the catalyst accurately. In particular, the methoxy groups attached to the naphthyl substituents interact with both of the substrates through C–H···O hydrogen bonds and/or C–H···π interactions. It is considered that these interactions contribute to the high enantioselectivity, despite the fact that these methoxy groups are distant from the activation site, because the use of catalyst (*R*)-**3d** having methoxy groups attached to a different position (7-position) of the naphthyl substituents resulted in the marked reduction of enantioselectivity (Table 1, entry 4). It is concluded that the combination of not only the steric congestion between the substrates and the catalyst but also these noncovalent bond interactions,[23] coupled with the structural distortion of the catalyst fragment (*vide infra*), is the key to differentiating the major and minor pathways. In order to gain an insight into the effectiveness of the perfluoro-binaphthyl skeleton, we next turned our attention to the structural properties of the catalysts by performing DFT calculations. For this purpose, we focused on the chiral phosphate anion (PA). The structural analysis of PAs was conducted as follows:[24] (i) the structure of F_{10}BINOL-derived phosphate anion (*R*)-**3PA$_{TS\text{-}s}$** was extracted from **TS-s** (Fig. 3a); (ii) the structure of F_{10}BINOL-derived phosphate anion (*R*)-**3PA$_{opt}$** was optimized from (*R*)-**3PA$_{TS\text{-}s}$** as the initial structure (Fig. 3b); and (iii) the structure of BINOL-derived phosphate anion (*R*)-**1PA$_{opt}$** was optimized after replacing the fluorine atoms of (*R*)-**3PA$_{opt}$** with hydrogen atoms (Fig. 3c). Then, we extracted the following key geometric parameters (Table 2): dihedral angles (C^2–C^1–C^a–C^b, $C^{2'}$–$C^{1'}$–$C^{a'}$–$C^{b'}$), interior bond angles (*A* and *A*′), and exterior bond angles (*B* and *B*′), which influence the distance between the 6-methoxy-2-naphthyl substituents of the catalyst and the substrates.[25]

As shown in Table 2, the dihedral angles C^2–C^1–C^a–C^b and $C^{2'}$–$C^{1'}$–$C^{a'}$–$C^{b'}$ in (*R*)-**3PA$_{TS\text{-}s}$** are markedly different from those in (*R*)-**3PA$_{opt}$**, whereas the dihedral angles in (*R*)-**3PA$_{opt}$** and (*R*)-**1PA$_{opt}$** show a little difference because of the influence of the substituted atoms at the 4,4′-positions. Considering these characteristics, the marked differences of the dihedral angles between (*R*)-**3PA$_{TS\text{-}s}$** and (*R*)-**3PA$_{opt}$** clearly indicate that the 6-methoxy-2-naphthyl substituents rotate to meet the requirements for the noncovalent bond interactions and the steric exclusion with the substrates in the transition state. In contrast, the interior bond angles *A* and *A*′ in (*R*)-**3PA$_{TS\text{-}s}$** are almost identical to those in (*R*)-**3PA$_{opt}$** and smaller than the ideal angle (120°). Hence, these bond angles are not affected by the substrates in the transition state but arise from the inherent structural characteristics of the perfluoro-binaphthyl skeleton. Indeed, the bond angles *A* and *A*′ of (*R*)-**3PA$_{opt}$** are smaller than those of (*R*)-**1PA$_{opt}$** of which angles are nearly ideal, probably due to the repulsion of fluorine atoms at the 8,8′-positions in (*R*)-**3PA$_{opt}$**. On the other hand, the exterior bond angles *B* and *B*′ in (*R*)-**3PA$_{opt}$** are slightly larger than those in (*R*)-**1PA$_{opt}$** presumably because of the repulsion between fluorine atoms at the 4,4′-positions and the naphthyl substituents at the 3,3′-positions.

The bond angle differences (Δ*A*, Δ*A*′, Δ*B*, and Δ*B*′) between (*R*)-**3PA$_{opt}$** and (*R*)-**1PA$_{opt}$** are not significant. However, these bond angles markedly influence the direction of the naphthyl substituents and hence the location of the tail end of the naphthyl substituents should be entirely different between (*R*)-**3PA$_{opt}$** and (*R*)-**1PA$_{opt}$**. Thus, in the F_{10}BINOL-derived catalyst having small *A* and *A*′ and large *B* and *B*′, the 6-methoxy-2-naphthyl substituents create a narrow reaction space inherently and hence approach the transition structure. Interestingly, further enlargement of the exterior bond angles *B* and *B*′ is observed in (*R*)-**3PA$_{TS\text{-}s}$**. This implies that the noncovalent bond interactions between the catalyst and the substrates, which stabilize the transition states, lead to structural distortion of the catalyst, although this distortion results in an energetic destabilization of the catalyst fragment. It is considered that F_{10}BINOL-derived phosphoric acid having an intrinsic narrow reaction space is allowed to interact with the transition structure of the substrates while minimizing catalyst distortion,

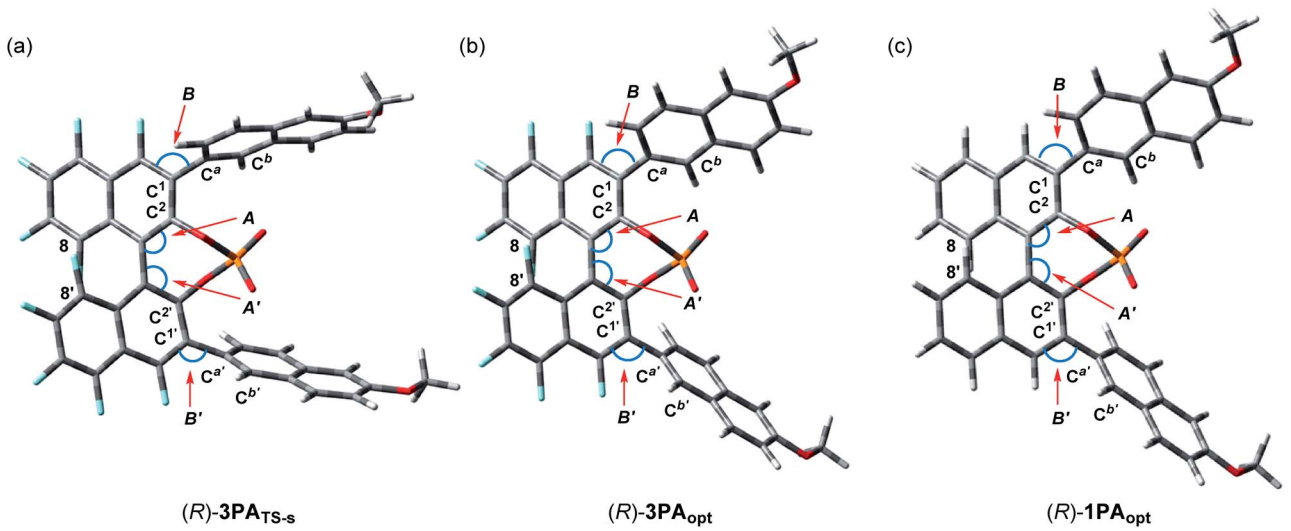

Fig. 3 Structural analysis of the catalysts. (a) F_{10}BINOL-derived phosphate anion from **TS-s**. (b) Optimized structure of F_{10}BINOL-derived phosphate anion (*R*)-3PA$_{opt}$. (c) Optimized structure of BINOL-derived phosphate anion (*R*)-1PA$_{opt}$.

Table 2 Selected geometric parameters for catalyst structures

	C^2–C^1–C^a–C^b	$C^{2'}$–$C^{1'}$–$C^{a'}$–$C^{b'}$	*A*	*A′*	*B*	*B′*
(*R*)-**3PA$_{TS\text{-}s}$**	76.4°	115.7°	118.0°	117.4°	122.8°	123.6°
(*R*)-**3PA$_{opt}$**	50.3°	134.4°	117.8°	117.2°	120.2°	121.7°
(*R*)-**1PA$_{opt}$**	46.0°	139.7°	119.1°	118.6°	119.5°	120.5°

namely, structural destabilization. In contrast, the BINOL-derived phosphoric acid framework creates a wide reaction space and hence the distortion should be more significant than that of the F_{10}BINOL-derived one, when a similar transition structure is formed through the noncovalent bond interactions between the substrates and the catalyst.[25] Consequently, the structural distortion of the catalyst, which results in the destabilization of the transition states, is also considered one of the rational factors for determining the stereochemical outcome (Scheme 2).[26]

Confirmation of potential of F_{10}BINOL-derived phosphoric acid

With the optimized catalyst and reaction conditions in hand, as shown in Table 1, the potential of F_{10}BINOL-derived phosphoric acid was further confirmed in the reaction that used a series of 1,1-disubstituted olefins having a cyclic framework. As shown in Table 3, the reaction of α-methylenetetralin derivatives **4b–g** having an electron-donating or -withdrawing group afforded the corresponding products **6** in moderate to good yields (entries 1–6). In addition, high enantioselectivities were observed in most cases, although **6c** and **6g** exhibited moderate enantioselectivities (entries 3 and 6). The decrease in enantioselectivity of **6g** suggests that the C–H bond at the C8 position is important to achieve high enantioselectivity. Indeed, as shown in the transition structure of the more favorable **TS-s** (Fig. 2a), C–H···O hydrogen bond is formed between the hydrogen atom at the C8 position and the phosphoryl oxygen of the catalyst. Notably, oxygen and sulfur heterocycles **4h** and **4i**, respectively, were compatible, affording the corresponding chromene **6h** and thiochromene **6i** derivatives with high enantioselectivities (entries 7 and 8). α-Methylenindane **4j** having a five-membered ring was also applicable to the reaction, although both yield and enantioselectivity were moderate (entry 9). The reaction of **4k** having a seven-membered ring furnished **6k** in an acceptable yield with the highest enantioselectivity among the olefins tested (entry 10). As shown in Table 1, entry 9 and Table 3, entries 9 and 10, an increase in the ring size of 1,1-disubstituted

Table 3 Scope of 1,1-disubstituted olefins[a]

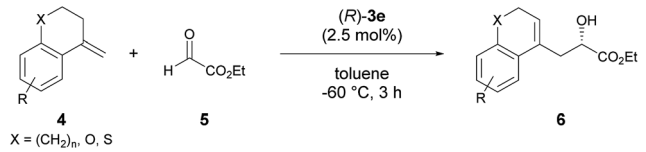

Entry	**4**		Yield[b] (%)	ee[c] (%)
1	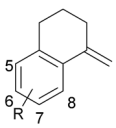	**4b**: R = 5-MeO	77	86
2		**4c**: R = 6-MeO	87	63
3		**4d**: R = 6-Cl	66	86
4		**4e**: R = 7-MeO	86	92
5		**4f**: R = 7-Br	64	88
6[d]		**4g**: R = 8-Br	37	60
7	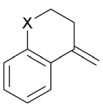	**4h**: X = O	75	91
8		**4i**: X = S	59	83
9	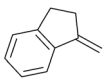	**4j**	48	62
10[e]	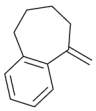	**4k**	75	93

[a] Unless otherwise noted, all reactions were carried out using 0.005 mmol of (*R*)-**3** (2.5 mol%), 0.2 mmol of **4**, and 0.4 mmol of **5** (2.0 eq.) in toluene (1.0 mL) at −60 °C. [b] Isolated yield. [c] ee was determined by chiral stationary phase HPLC analysis. [d] Reaction was conducted at −40 °C. [e] 0.6 mmol of **5** was used.

olefins from five to seven markedly enhanced the enantioselectivity from 62% ee (five) to 93% ee (seven) *via* 87% ee (six). This trend is also well rationalized on the basis of the transition structures of the present reaction (Fig. 2). In the more favorable **TS-s**, ene-component **4a** and enophile **5** are nearly parallel to the naphthyl planes of the catalyst substituents and hence the ring size does not cause steric congestion between ene-component **4** and the naphthyl substituents. In contrast, in the less favorable **TS-r**, **4a** and **5** are perpendicular to the two naphthyl substituents. Therefore, the increase in ring size enhances the repulsive interaction between ene-component **4** and the naphthyl substituents, which leads to further destabilization of the transition state in the minor pathway. The enhancement of enantioselectivity with increasing ring size is rationally understood on the basis of the above structural expectations in these transition states.

Conclusions

We have demonstrated that F_{10}BINOL-derived chiral phosphoric acid is an effective catalyst for the enantioselective carbonyl-ene reaction. This highly acidic catalyst efficiently activated ethyl glyoxylate as the common enophile and accelerated the reaction with 1,1-disubstituted olefins, affording the corresponding homoallylic alcohols in good yields with high enantioselectivities in most cases. Theoretical studies of the present catalytic reaction revealed that multi-point noncovalent bond interactions, such as O···H···O, C–H···O hydrogen bonds, C–H···π, and π–π stacking, determine the relative locations of the catalyst and the substrates, namely, the enophile and the ene-component, accurately. In fact, it was confirmed that the remote noncovalent bond interactions between the substrates and the methoxy groups introduced to the naphthyl substituents of the catalyst aid to stabilize the transition structures. Further structural analysis of F_{10}BINOL-derived catalyst identified the specific properties of the F_{10}BINOL skeleton. The introduction of fluorine atoms to the binaphthyl skeleton leads to bond angle distortion, which induces the 6-methoxy-2-naphthyl substituents to create a narrow reaction space for the transition structure. The higher enantioselectivity achieved by F_{10}BINOL-derived phosphoric acid than by BINOL-derived ones originates from this narrow reaction space in which noncovalent bond interactions occur readily without marked distortion, namely, destabilization, of the catalyst framework and stabilize the transition states efficiently in the major pathway. Based on these theoretical studies of the transition states and the structural analysis of the catalyst frameworks, it is concluded that the major and minor pathways are differentiated by the total balance of the steric congestion between the substrates and the catalyst, the noncovalent bond interactions, and the structural distortion of the catalyst framework. Further studies of the development of enantioselective reactions using F_{10}BINOL-derived chiral Brønsted acids will be conducted in due course.

Conflicts of interest

There are no conflicts to declare.

Acknowledgements

This work was partially supported by a Grant-in-Aid for Scientific Research on Innovative Areas "Advanced Molecular Transformations by Organocatalysts" from The MEXT, Japan (No. 23105002) and a Grant-in-Aid for Scientific Research on Innovative Areas "Hybrid Catalysis for Enabling Molecular Synthesis on Demand" from the MEXT, Japan (No. JP17H06447). We gratefully thank Professor Toshinobu Korenaga (Department of Chemistry and Biological Sciences, Faculty of Science and Engineering, Iwate University) for his helpful advice of the theoretical studies.

Notes and references

1 For selected reviews on chiral Brøsnted acid catalysis, see: (*a*) T. Akiyama, *Chem. Rev.*, 2007, **107**, 5744–5758; (*b*) M. Terada, *Synthesis*, 2010, 1929–1982; (*c*) D. Kampen, C. M. Reisinger and B. List, *Top. Curr. Chem.*, 2010, **291**, 395–456; (*d*) D. Parmar, E. Sugiono, S. Raja and M. Rueping, *Chem. Rev.*, 2014, **114**, 9047–9153.

2 For book and reviews on enantioselective organocatalysis, see: (*a*) P. I. Dalko and L. Moisan, *Angew. Chem., Int. Ed.*, 2004, **43**, 5138–5175; (*b*) J. Seayad and B. List, *Org. Biomol. Chem.*, 2005, **3**, 719–724; (*c*) B. List, *Chem. Commun.*, 2006, 819–824; (*d*) M. S. Taylor and E. N. Jacobsen, *Angew. Chem., Int. Ed.*, 2006, **45**, 1520–1543; (*e*) *Enantioselective Organocatalysis: Reactions and Experimental Procedures*, ed. P. I. Dalko, Wiley-VCH, Weinheim, 2007; (*f*) N. Marion, S. Díez-González and S. P. Nolan, *Angew. Chem., Int. Ed.*, 2007, **46**, 2988–3000; (*g*) R. M. de Figueiredo and M. Christmann, *Eur. J. Org. Chem.*, 2007, 2575–2600; (*h*) H. Pellissier, *Tetrahedron*, 2007, **63**, 9267–9331; (*i*) A. G. Doyle and E. N. Jacobsen, *Chem. Rev.*, 2007, **107**, 5713–5743.

3 Seminal works of chiral phosphoric acid, see: (*a*) T. Akiyama, J. Itoh, K. Yokota and K. Fuchibe, *Angew. Chem., Int. Ed.*, 2004, **43**, 1566–1568; (*b*) D. Uraguchi and M. Terada, *J. Am. Chem. Soc.*, 2004, **126**, 5356–5357.

4 (*a*) D. Nakashima and H. Yamamoto, *J. Am. Chem. Soc.*, 2006, **128**, 9226–9627; (*b*) T. Hashimoto and K. Maruoka, *J. Am. Chem. Soc.*, 2007, **129**, 10054–10055; (*c*) M. Hatano, T. Maki, K. Moriyama, M. Arinobe and K. Ishihara, *J. Am. Chem. Soc.*, 2008, **130**, 16858–16860; (*d*) P. García-García, F. Lay, P. García-García, C. Rabalakos and B. List, *Angew. Chem., Int. Ed.*, 2009, **48**, 4363–4366; (*e*) I. Čorić and B. List, *Nature*, 2012, **483**, 315–319.

5 (*a*) D. J. Morrison, S. D. Riegel, W. E. Piers, M. Parvez and R. McDonald, *Chem. Commun.*, 2006, 2875–2877; (*b*) N. Momiyama, H. Okamoto, M. Shimizu and M. Terada, *Chirality*, 2015, **27**, 464–475.

6 N. Momiyama, H. Okamoto, J. Kikuchi, T. Korenaga and M. Terada, *ACS Catal.*, 2016, **6**, 1198–1204.

7 For enantioselective imino-ene reactions, see: (*a*) W. J. Drury III, D. Ferraris, C. Cox, B. Young and T. Lectka, *J. Am. Chem. Soc.*, 1998, **120**, 11006–11007; (*b*) S. Yao, X. Fang and K. A. Jørgensen, *Chem. Commun.*, 1998, 2547–2548; (*c*)

D. Ferraris, B. Young, C. Cox, T. Dudding, W. J. Drury III, L. Ryzhkov, A. W. Taggi and T. Lectka, *J. Am. Chem. Soc.*, 2002, **124**, 66–67; (*d*) N. A. Caplan, F. E. Hancock, P. C. B. Page and G. H. Hutchings, *Angew. Chem., Int. Ed.*, 2004, **43**, 1685–1688; (*e*) M. Hatano, K. Nishikawa and K. Ishihara, *J. Am. Chem. Soc.*, 2017, **139**, 8424–8427.

8 In order to estimate the acidity of (*R*)-**3a** (Ar = Ph), we conducted the DFT-calculation in accordance with Cheng's methods. The calculated pK_a value of (*R*)-**3a** (Ar = Ph) in DMSO: 1.24 (proton exchange method), 1.03 (direct method). See ESI† for details. Cheng *et al.* calculated the pK_a value of (*R*)-**1** (Ar = Ph) and (*R*)-**2** (Ar = Ph)(*a*) pK_a value of (*R*)-**1**C. Yang, X.-S. Xue, J.-L. Jin, X. Li and J.-P. Cheng, *J. Org. Chem.*, 2013, **78**, 7076–7085 (Ar = Ph) in DMSO: 3.55 (proton exchange method), 3.33 (direct method), see: ; (*b*) pK_a value of (*R*)-**2** (Ar = Ph) in DMSO: −3.36 (direct method), see: C. Yang, X.-S. Xue, X. Li and J.-P. Cheng, *J. Org. Chem.*, 2014, **79**, 4340–4351.

9 B. M. Trost, *Angew. Chem., Int. Ed. Engl.*, 1995, **34**, 259–281.

10 For selected examples of enantioselective carbonyl-ene reactions, see: (*a*) K. Maruoka, Y. Hoshino, T. Shirasaka and H. Yamamoto, *Tetrahedron Lett.*, 1988, **29**, 3967–3970; (*b*) K. Mikami, M. Terada and T. Nakai, *J. Am. Chem. Soc.*, 1989, **111**, 1940–1941; (*c*) D. A. Evans, C. S. Burgey, N. A. Paras, T. Vojkovsky and S. W. Tregay, *J. Am. Chem. Soc.*, 1998, **120**, 5824–5825; (*d*) C. Qian and L. Wang, *Tetrahedron: Asymmetry*, 2000, **11**, 2347–2357; (*e*) S. Kezuka, T. Ikeno and T. Yamada, *Org. Lett.*, 2001, **3**, 1937–1939; (*f*) J. H. Koh, A. O. Larsen and M. R. Gagné, *Org. Lett.*, 2001, **3**, 1233–1236; Y. Yuan, X. Zhang and K. L. Ding, *Angew. Chem., Int. Ed.*, 2003, **42**, 5478–5480. (*g*) G. E. Hutson, A. H. Dave and V. H. Rawal, *Org. Lett.*, 2007, **9**, 3869–3872; (*h*) M. L. Grachan, M. T. Tudge and E. N. Jacobsen, *Angew. Chem., Int. Ed.*, 2008, **47**, 1469–1472; (*i*) K. Zheng, J. Shi, X. Liu and X. M. Feng, *J. Am. Chem. Soc.*, 2008, **130**, 15770–15771; (*j*) P. M. Truong, P. Y. Zavalij and M. P. Doyle, *Angew. Chem., Int. Ed.*, 2014, **53**, 6468–6472; (*k*) X. C. Xu, X. C. Wang, Y. Liu and M. P. Doyle, *J. Org. Chem.*, 2014, **79**, 12185–12190; (*l*) X. Zhang, M. Wang, R. Ding, Y.-H. Xu and T.-P. Loh, *Org. Lett.*, 2015, **17**, 2736–2739.

11 (*a*) M. Rueping, T. Theissmann, A. Kuenkel and R. M. Koenigs, *Angew. Chem., Int. Ed.*, 2008, **47**, 6798–6801; (*b*) L. Liu, M. Leutzsch, Y. Zheng, M. W. Alachraf, W. Thiel and B. List, *J. Am. Chem. Soc.*, 2015, **137**, 13268–13271; (*c*) J. Lv, Q. Zhang, X. Zhong and S. Luo, *J. Am. Chem. Soc.*, 2015, **137**, 15576–15583.

12 The enantioselective carbonyl-ene reaction of α-methylstyrene was also attempted in the presence of 2.5 mol% (*R*)-**3e**. Although the reaction gave a product with excellent enantioselectivity, the yield was extremely low (5% yield, 90% ee). See ESI† for details.

13 For selected recent reports of theoretical studies on stereochemical outcomes using chiral phosphoric acids, see: (*a*) Y. Y. Khomutnyk, A. J. Argüelles, G. A. Winschel, Z. Sun, P. M. Zimmerman and P. Nagorny, *J. Am. Chem. Soc.*, 2016, **138**, 444–456; (*b*) J. P. Reid and J. M. Goodman, *J. Am. Chem. Soc.*, 2016, **138**, 7910–7917; (*c*) R. Maji, P. A. Champagne, K. N. Houk and S. E. Wheeler, *ACS Catal.*, 2017, **7**, 7332–7339.

14 M. J. Frisch, *et al.*, *Gaussian 16, Revision B.01*, Gaussian, Inc., Wallingford, CT, 2016, see ESI† for the full citation.

15 For M06-2X, see: Y. Zhao and D. G. Truhlar, *Theor. Chem. Acc.*, 2008, **120**, 215–241.

16 For Gaussian basis sets, see: (*a*) M. J. Frisch, J. A. Pople and J. S. Binkley, *J. Chem. Phys.*, 1984, **80**, 3265–3269; (*b*) W. J. Hehre, L. Radom, P. v. R. Schleyer and J. A. Pople, *Ab initio Molecular Orbital Theory*, John Wiley, New York, USA, 1986, and references cited therein.

17 For the CPCM model, see: (*a*) V. Barone and M. Cossi, *J. Phys. Chem. A*, 1998, **102**, 1995–2001; (*b*) B. Barone, M. Cossi and J. Tomasi, *J. Comput. Chem.*, 1998, **19**, 404–417.

18 In order to conduct rigorous conformational analysis of these transition states, initial structures of the transition states were systematically generated by changing the dihedral angles of C^2–C^1–C^a–C^b and $C^{2'}$–$C^{1'}$–$C^{a'}$–$C^{b'}$ (for each dihedral angle: −135°, −45°, 45°, and 135°) as well as the orientation of the methoxy group (dihedral angle: 0° and 180° to the naphthyl ring). This procedure generates eight conformers for each naphthyl ring and hence totally 64 conformers were considered for the initial structures of the catalyst. In addition, on the basis of the model studies of the transition states, conformationally different transition states of the real system were considered by changing the orientation of ene-component **4a** and the conformation of the six-membered ring of **4a** for each enantiomeric pathway. Thus, nearly 200 initial structures were calculated to identify the energetically favored transition states accurately.

19 The ee value was calculated as follows: $\mathrm{ee} = \dfrac{\exp\left(\dfrac{\Delta\Delta G^{TS}}{RT}\right) - 1}{\exp\left(\dfrac{\Delta\Delta G^{TS}}{RT}\right) + 1}$, where $\Delta\Delta G^{TS}$ is the energy gap between major and minor transition states, R is the gas constant, and T is the absolute temperature. The 1.1 kcal mol^{-1} energy gap at −60 °C corresponds to 86% ee.

20 For representative and recent examples for C–H···O hydrogen bonds as the key interaction in asymmetric catalysis, see: (*a*) E. J. Corey and J. J. Rohde, *Tetrahedron Lett.*, 1997, **38**, 37–40; (*b*) M. N. Grayson and J. M. Goodman, *J. Am. Chem. Soc.*, 2013, **135**, 6142–6148; (*c*) P. Maity, R. P. Pemberton, D. J. Tantillo and U. K. Tambar, *J. Am. Chem. Soc.*, 2013, **135**, 16380–16383; (*d*) H. Wang, P. Jain, J. C. Antilla and K. N. Houk, *J. Org. Chem.*, 2013, **78**, 1208–1215; (*e*) T. Ishii, R. Watanabe, T. Moriya, H. Ohmiya, S. Mori and M. Sawamura, *Chem.–Eur. J.*, 2013, **19**, 13547–13553; (*f*) K. Kanomata, Y. Toda, Y. Shibata, M. Yamanaka, S. Tsuzuki, I. D. Gridnev and M. Terada, *Chem. Sci.*, 2014, **5**, 3515–3523; (*g*) N. Grimblat, M. Sugiura and S. C. Pellegrinet, *J. Org. Chem.*, 2014, **79**, 6754–6758; (*h*) Y. Xie, G.-J. Cheng, S. Lee, P. S. J. Kaib, W. Thiel and B. List, *J. Am. Chem. Soc.*, 2016, **138**, 14538–14541; (*i*) M. N. Grayson, Z. Yang and K. N. Houk, *J. Am.*

Chem. Soc., 2017, **139**, 7717–7720; (*j*) Y. Takayama, T. Ishii, H. Ohmiya, T. Iwai, M. C. Schwarzer, S. Mori, T. Taniguchi, K. Monde and M. Sawamura, *Chem.–Eur. J.*, 2017, **23**, 8400–8404; (*k*) F. Li, T. Korenaga, T. Nakanishi, J. Kikuchi and M. Terada, *J. Am. Chem. Soc.*, 2018, **140**, 2629–2642.

21 For π interactions, see: (*a*) E. H. Krenske and K. N. Houk, *Acc. Chem. Res.*, 2013, **46**, 979–989; (*b*) A. J. Neel, M. J. Hilton, M. S. Sigman and F. D. Toste, *Nature*, 2017, **543**, 637–646.

22 For representative and recent examples of π interaction as the key interaction in asymmetric catalysis, see: (*a*) M. Yamakawa, I. Yamada and R. Noyori, *Angew. Chem., Int. Ed.*, 2001, **40**, 2818–2821; (*b*) H. Kawai, A. Kusuda, S. Nakamura, M. Shiro and N. Shibata, *Angew. Chem., Int. Ed.*, 2009, **48**, 6324–6327; (*c*) J. Calleja, A. B. Gonzalez-Perez, A. R. de Lera, R. Alvarez, F. J. Fanan and F. Rodrıguez, *Chem. Sci.*, 2014, **5**, 996–1007; (*d*) G. Jindal and R. B. Sunoj, *Angew. Chem., Int. Ed.*, 2014, **53**, 4432–4436; (*e*) S. S. Meng, Y. Liang, K. S. Cao, L. Zou, X. B. Lin, H. Yang, K. N. Houk and W. H. Zheng, *J. Am. Chem. Soc.*, 2014, **136**, 12249–12252; (*f*) B. Bhaskararao and R. B. Sunoj, *J. Am. Chem. Soc.*, 2015, **137**, 15712–15722; (*g*) A. C. Doney, B. J. Rooks, T. X. Lu and S. E. Wheeler, *ACS Catal.*, 2016, **6**, 7948–7955; (*h*) M. Pareek and R. B. Sunoj, *ACS Catal.*, 2016, **6**, 3118–3126; (*i*) J. Guo and M. W. Wong, *J. Org. Chem.*, 2017, **82**, 4362–4368; (*j*) M. Li and X.-S. Xue, *ACS Catal.*, 2017, **7**, 7977–7986; (*k*) T. Korenaga, R. Sasaki, T. Takemoto, T. Yasuda and M. Watanabe, *Adv. Synth. Catal.*, 2018, **360**, 322–333.

23 The second-order perturbative donor–acceptor interactions for the two transition states were also analyzed. See ESI† for details.

24 The structures of the catalysts were optimized as phosphate anion because the acidic proton is located closer to enophile **5** than the catalyst fragment in **TS-s**. For the optimization of the catalyst structures as phosphoric acid, see ESI† for details.

25 The same structural analysis of BINOL-derived phosphate anion (*R*)-$\mathbf{1PA_{TS\text{-}s}}$, which was extracted from the transition state of the major pathway of the carbonyl-ene reaction catalyzed by (*R*)-**1** (Ar = 6-methoxy-2-naphthyl), was also conducted. It has been confirmed that the structural distortion of the BINOL-derived phosphoric acid framework is more significant than that of the F10BINOL-derived one. See ESI† for details.

26 For the distortion/interaction analysis of transition states, see: (*a*) K. Morokuma, and K. Kitaura, in *Chemical Applications of Atomic and Molecular Electrostatic Potentials*, ed. P. Politzer and D. G. Truhlar, Plenum press, New York, 1981, pp. 215−242; (*b*) D. H. Ess and K. N. Houk, *J. Am. Chem. Soc.*, 2007, **129**, 10646–10647; (*c*) D. H. Ess and K. N. Houk, *J. Am. Chem. Soc.*, 2008, **130**, 10187–10198; (*d*) Y.-H. Lam, P. H.-Y. Cheong, J. M. Blasco Mata, S. J. Stanway, V. Gouverneur and K. N. Houk, *J. Am. Chem. Soc.*, 2009, **131**, 1947–1957; (*e*) R. S. Paton, S. Kim, A. G. Ross, S. J. Danishefsky and K. N. Houk, *Angew. Chem., Int. Ed.*, 2011, **50**, 10366–10368; (*f*) A. G. Green, P. Liu, C. A. Merlic and K. N. Houk, *J. Am. Chem. Soc.*, 2014, **136**, 4575–4583; (*g*) F. M. Bickelhaupt and K. N. Houk, *Angew. Chem., Int. Ed.*, 2017, **56**, 10070–10086.